Deformation experiments in the diamond-anvil cell: texture in copper to 30 GPa

2006 J. Phys.: Condens. Matter 18 S1007

(http://iopscience.iop.org/0953-8984/18/25/S08)

INSTITUTE OF PHYSICS PUBLISHING JOURNAL OF PHYSICS: CONDENSED MATTER

J. Phys.: Condens. Matter **18** (2006) S1007–S1020 doi:10.1088/0953-8984/18/25/S08

Deformation experiments in the diamond-anvil cell: texture in copper to 30 GPa

S Speziale, I Lonardelli, L Miyagi, J Pehl, C E Tommaseo and H-R Wenk

Department of Earth and Planetary Science, University of California, Berkeley, CA 94720, USA

E-mail: speziale@uclink.berkeley.edu

Received 2 December 2005, in final form 3 March 2006
Published 8 June 2006
Online at stacks.iop.org/JPhysCM/18/S1007

Abstract

The combination of the diamond-anvil cell, synchrotron x-ray diffraction in radial geometry and simultaneous Rietveld refinement with texture analysis allows us to quantitatively investigate the plastic deformation behaviour of materials at very high pressures. Our study of copper to 30 GPa shows in ideal experimental geometry a [110] fibre texture component, as is typical for axial compression of soft face centred cubic metals. Locally a plane strain texture develops which is energetically favoured (curling). A transition from compressional to plane strain/pure shear texture can be monitored by analysing individual images taken at different positions in the diamond cell.

1. Introduction

The diamond-anvil cell (DAC) and synchrotron x-ray diffraction allow the study of mechanical properties of materials at extremely high pressures [1, 2]. Radial x-ray diffraction at high pressure [3–6] has been developed to investigate the elasticity and strength of solids at extreme conditions. Recent developments of gasket technology [7, 8] combined with angle-dispersive experimental geometry [6] make it possible to study the deformation of minerals, up to pressures comparable to the lower mantle [9]. The geophysical materials of interest for understanding the rheology of the deep interior of the Earth are mainly silicate oxides which are often thermodynamically unstable at ambient conditions, so their physical properties can only be studied at high pressures in side the diamond-anvil cell where they are synthesized.

In order to investigate the strain geometry in the diamond cell, we have performed experiments on copper, a reference material both in high-pressure solid state physics and in materials science, for which numerous results are available from both static compression (e.g. [10, 11]) and dynamic compression experiments (see [12] for a review) in a wide range of pressure and temperature conditions. Metallurgists have established texture development and deformation mechanisms in face centred cubic (fcc) metals (e.g. [13] and references within). The deformation behaviour of copper at moderate to high stress levels has long been studied and modelled under low confining pressure (e.g. [14]). In addition, the equation of state of

Table 1. Conditions attained in the different experimental runs.

Experiment	Initial sample diameter (μm)	Max. pressure (GPa)	Final sample geometry
Copper-1	80	30 ± 2	Contained in the chamber
Copper-2	80	27 ± 2	Contained in the chamber
Copper-3	80	24 ± 2	Contained in the chamber
Copper-4	80	21 ± 2	Extruded (normal to x-ray)
Copper-5	80	8–29	Extruded (parallel to x-ray)

this metal, based on a large number of experimental data collected with different techniques, is known with high accuracy across a very large pressure–temperature range [11, 15]. These characteristics make copper a good material to test the accuracy of the data analysis and reproducibility of the high-pressure deformation technique of DAC radial x-ray diffraction experiments. The reproducibility and accuracy of texture determination is tested in this study by performing multiple experiments in the same pressure range. Tests of texture homogeneity are also performed in the different experiments, by collecting x-ray diffraction spectra from different regions of the sample. This investigation was originally motivated by the observation of strange texture patterns for gold, used as the pressure calibrant in previous experiments with oxides and silicates [9].

2. Materials and methods

High-purity copper powder (99.9% purity, from Alfa Aesar) of average 3–5 μm grain-size was pressed to form a 10 μm thick foil. Fragments of the foil were loaded in 90 μm wide sample chambers drilled in composite gaskets made of a boron–epoxy central disc of 400 μm diameter and 60 μm thickness, surrounded by a Kapton® (DuPont) confining ring 120 μm thick [8]. The initial size of the coherently scattering crystalline domains was estimated to be about 0.3 μm at the beginning of the experiments by Rietveld analysis of x-ray diffraction images of copper at ambient conditions.

The samples were compressed between diamond culets of 300 μm diameter. A fragment of gold foil (15–20 μm diameter, 5–10 μm thickness) was loaded together with copper and used as position marker and pressure calibrant in each experiment. The gold foil was prepared by pressing gold powder from Alfa Aesar (99.95% pure) of average 5 μm grain-size. The fragment of gold was carefully positioned within 5–10 μm from the centre of both the sample and the diamond culet face.

All the x-ray diffraction experiments were performed in radial geometry using monochromatic synchrotron radiation and image plate detectors. The compression direction, corresponding to the axis of the diamond anvils, was horizontal in all the experiments, i.e. the sample radial direction was the vertical direction.

Experiments 1 to 3 (Copper-1 to Copper-3; see table 1) were performed at beamline 13BM-D of the GeoSoilEnviro-Consortium for Advanced Radiation Sources (GSECARS) at the Advanced Photon Source (APS) of Argonne National Laboratory (Argonne, IL) using monochromatic x-rays with a wavelength of 0.309 91 Å, focused to a 18 μm (vertical) $\times$ 7 μm (horizontal) spot size, and a Mar345 image plate detector. The sample to detector distance was fixed at 426 mm. In these experiments the samples were compressed in a standard piston–cylinder diamond anvil cell [5] with 29° lateral opening.

Experiment 4 (Copper-4) was performed at beamline 16ID-B of the High Pressure Collaborative Access Team (HPCAT) at the APS, using monochromatic x-rays with a

wavelength of 0.4325 Å, focused to a size of 10 μm × 10 μm, and a Mar345 image plate detector. The sample to detector distance was fixed at 348 mm. The sample was compressed in a panoramic piston–cylinder diamond-anvil cell [16] with 68° lateral opening.

Experiment 5 (Copper-5) was performed at the new high-pressure beamline 12.2.2 of the Advanced Light Source (ALS) of Lawrence Berkeley National Laboratory (Berkeley, CA) [17]. We used monochromatic radiation with a wavelength of 0.4959 Å, focused to a size of less than 20 μm × 20 μm, and a Mar345 image plate detector. The sample to detector distance was 414 mm. In this experiment we used a panoramic piston–cylinder diamond-anvil cell as in experiment 4. The names of the experimental runs, the initial sample geometry and the maximum pressure achieved in the experiments are reported in table 1.

3. Data analysis

The x-ray diffraction images collected in radial geometry were analysed first by using the software Fit2d [18]. The sample to detector distance and the direct beam position were refined from a diffraction image of a standard material at ambient conditions (CeO_2 for both the experiments performed at beamlines 13BM-D and 16ID-B at the APS, and LaB_6 for the experiments conducted at beamline 12.2.2 of the ALS). Then, the 2D images were divided into circular sectors of 5° width and subsequently the sectors were integrated to obtain sequences of one-dimensional spectra. Due to the limited width of the lateral opening in the symmetric DACs used in the experiments Copper-1, 2, and 3, the sequences consisted of 33–36 individual 1D spectra extended to the 220 reflection (d-spacing range: 2.5–1.3 Å) with the addition of 24–28 spectra extended to the 311 reflection (d-spacing range: 2.5–1.02 Å). In the case of the experiments Copper-4 and 5, we used 72 spectra extended to the 222 reflection (d-spacing range: 2.5–1.02 Å).

For each image the sequence of 1D spectra was simultaneously analysed to extract both structural and textural information by using the software MAUD [19] that carries out both whole spectrum structural refinement [20] and texture analysis with the E-WIMF algorithm [21] extracting a model of the orientation distribution (OD). The resolution of the OD was fixed at 15° and the tube projection diameter was 30°. Details of the data processing and analysis are reported in [22]. We performed structural and texture analysis on single x-ray diffraction images, which can be sufficient to furnish complete textural information [23]. One example of an x-ray diffraction image and Rietveld fit result is shown in figure 1. The quality of the spectra fitting is well represented in the form of 2D maps of the calculated and observed intensities, obtained by stacking the sequence of spectra integrated across the azimuthal angle (figure 2(a)). Quantitative textural information is displayed by equiareal pole figure (figure 2(b)) calculated from the OD and oriented with the compression direction corresponding to the centre of the pole figures. In addition to the pole figures, inverse pole figures of the compression direction (i.e. projections of the compression direction referred to the crystal reference frame) are calculated in the case of experiments in which the ideal experimental geometry was preserved up to the highest pressure (experiments Copper-1, 2, and 3).

The experimental pressure, defined as the hydrostatic part of the macrostress applied to the sample, was estimated by applying a triaxial stress model to the diffraction data of gold and copper assuming that both the sample and the gold marker behave as effective elastically isotropic media. To convert the measured elastic strain of gold into stress we used the parameters of the isothermal equation of state from [24] and the shear modulus from [25]. Whenever a gold signal was not detected we estimated the pressure from the data for copper, using the parameters of the equation of state from [15] and the shear modulus from [26]. In the case of both gold and copper, the high-pressure elastic moduli were calculated using third-order

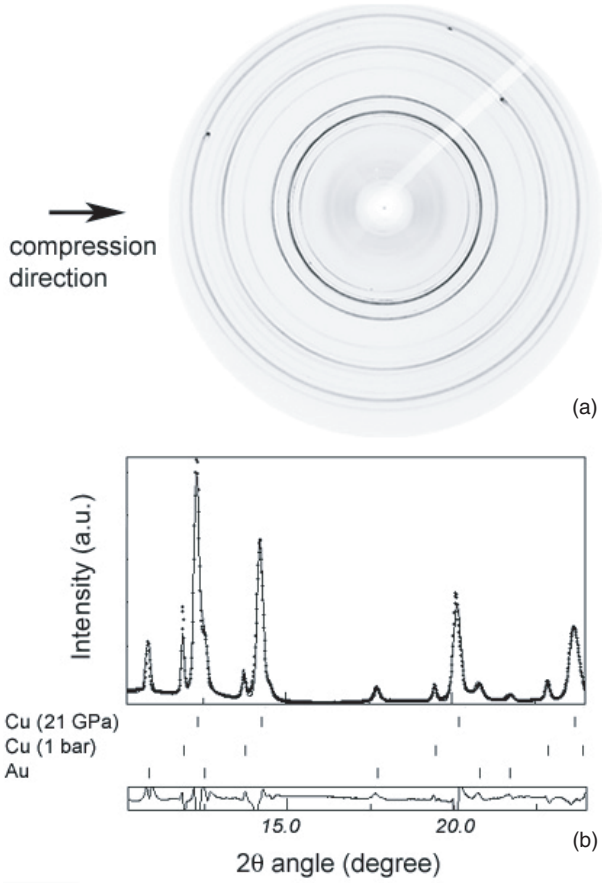

Figure 1. (a) Example of 2D x-ray diffraction image from experiment Copper-4. (b) Results of Rietveld refinement in the form of a calculated 1D diffraction spectrum (line) plot together with the observed spectrum (dots). Fitted residuals are reported at the bottom of the spectrum. In this experiment a signal from copper powder outside the sample chamber (at ambient pressure) was also detected.

Table 2. Examples of quantitative whole spectrum texture analysis of experiments 1, 2, and 3.

Experiment	Pressure (Cu) (GPa)	Pressure (Au) (GPa)	Deviatoric stress (GPa)	Min–max texture intensity[a] (mrd)	Texture index (F_2)[b]
Copper-1	24 ± 2	24 ± 2	0.2	0.5–2.0	1.6
Copper-2	16 ± 2	16 ± 2	0.2	0.5–2.0	1.8
Copper-3	24 ± 2	21 ± 2	0.3	0.6–2.6	3.7

[a] Minimum and maximum texture intensity expressed as pole density.
[b] Defined as the volume averaged integral of squared orientation density across the orientation distribution function [38].

Eulerian finite strain equations (e.g. [27]). The results for gold are in excellent agreement with those for copper in all the measurements in which a gold signal was detected (table 2).

A more restrictive set of assumptions [28] including perfect cylindrical symmetry of the applied stress ($\sigma_{33} > \sigma_{11} = \sigma_{22}$, where σ_{ii} are the principal components of the applied stress

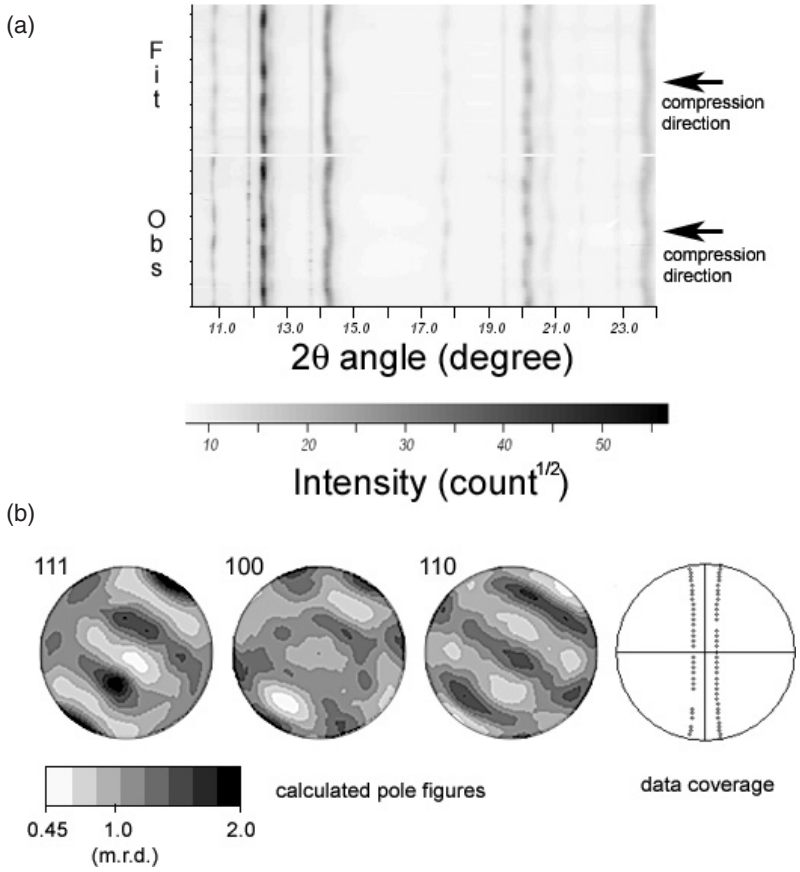

Figure 2. (a) Results of Rietveld texture refinement represented as a map plot of the calculated 1D spectra compared with the observed spectra. (b) Experimental data coverage (on the right) and calculated (111), (100) and (110) pole figures calculated from the OD (equal area projection). The compression direction is normal to the pole figures. The map plot and pole figures refer to the data of the 2D diffraction image in figure 1.

tensor) could be applied only to data collected from the centre of the sample when the applied stress has ideal axial symmetry, such as in our measurements taken at the centre of the sample in the experiments Copper-1, Copper-2 and Copper-3. We apply both the simple triaxial stress and the more restrictive cylindrically symmetric stress model to all the measurements from Copper-1, Copper-2, Copper-3, and Copper-4 presented in this study. In absence of a better model of the actual stress–strain conditions, we observe that the differences between the two methods are of the order of 0.1–1 GPa, which is systematically smaller than the average 1–2 GPa effective deviatoric stress inferred from the lattice strain variation (maximum deviation of d-spacing for the diffracting lattice planes) measured in each diffraction image from Copper-1, 2, 3 and Copper-4. For this reason we consider that 2 GPa represents a reasonable estimate of the uncertainty of the pressure determination in all the experimental results from Copper-1 to Copper-4 reported in this study.

In the case of Copper-5, the large peak broadening indicates a large pressure gradient in the sample. Accurate modelling of the stress conditions in the sample chamber is required to interpret the variation in elastic strain observed in the sample. A summary of the conditions

attained in the different experiments and of the final geometry of the samples is reported in table 1.

4. Texture results and discussion

4.1. Experiments in ideal compression geometry

The experiments Copper-1, 2, and 3 covered a wide pressure range up to a maximum of 30 GPa (Copper-1). The experimental geometry, monitored by x-ray transmission scans and by optical microscopy observation, was ideal throughout the whole experiment in each of the three experiments. The three experiments were performed with symmetric diamond-anvil cells that have limited lateral conical apertures (29°) for radial x-ray diffraction. In order to increase the maximum accessible 2θ we rotated the cell 5° around an axis perpendicular to the axis of the conical apertures. As a consequence only the 111 Debye diffraction ring is completely recorded in experiments 1, 2 and 3 and only a portion of the 200, 220 and 311 diffraction rings are measured. The limited data coverage may limit our ability to reconstruct the OD from our experimental results. The results of the texture analysis of the central portion of the three samples (Copper-1, 2, and 3) at the pressures of 24 $\pm$ 2 GPa, 16 $\pm$ 2 GPa, and 24 $\pm$ 2 GPa, respectively, are summarized in table 2 and displayed in figure 3 in the form of both experimental data coverage, (111), (100), and (110) pole figures calculated from the OD without imposing any sample symmetry, and inverse pole figures of the compression direction.

In all three cases the (110) poles tend to align parallel to the compression direction (figure 3), in agreement with the existing data for copper compressed at ambient temperature and subject to large strain. However, the inverse pole figures of the compression direction show that the [110] maximum systematically broadens towards [001] (figure 3). Some features of the pole figures, such as the inhomogeneous intensity of the high pole density girdle in the (111) pole figure (e.g. figure 3(c)), are more compatible with a rolling texture (e.g. [13] and references within). In fact, copper grains in the sample chamber are mainly aligned with [110] fibre components, but the deformation style locally departs from the ideal homogeneous axisymmetric compression towards plane strain because of the anisotropic mechanical properties of the fcc structure. Planes orthogonal to ⟨110⟩ do not allow the development of axially symmetric shape around ⟨110⟩ by means of {111} slip, which is the principal active system in copper. Compatibility across grain boundaries (physical continuity of the deformed material) causes 'curling', i.e. local adjustments of the grains' shape and orientation, and has long been known by metallurgists [29]. The resulting overall texture appears to be axially symmetric as a result of a 'rotational average' of the textures of different groups of crystals which locally deform in plane strain pure shear.

In addition to the standard measurements of radial x-ray diffraction from the central region of the samples we have also performed radial scans of the samples to investigate the homogeneity of texturing in the sample chamber. The results that we obtain from Copper-1, 2 and 3 at different pressures are in mutual agreement. As an example the texture along sample 1 at a pressure of 24 $\pm$ 2 GPa is shown in figure 4 as a sequence of (111), (200), (220) experimental pole figures and the corresponding (111), (100) and (110) recalculated pole figures extracted from data collected at different positions (r) across the radial extension of the sample. Numerical results of the texture analysis are summarized in table 3. Moving from the centre to the periphery of the sample, we notice a continuous change of the pattern of preferred orientation from apparently axially symmetric at the sample centre ($r = 0$) to plane strain texture at the edge of the sample ($r = 60$ μm). Local departure from axisymmetric

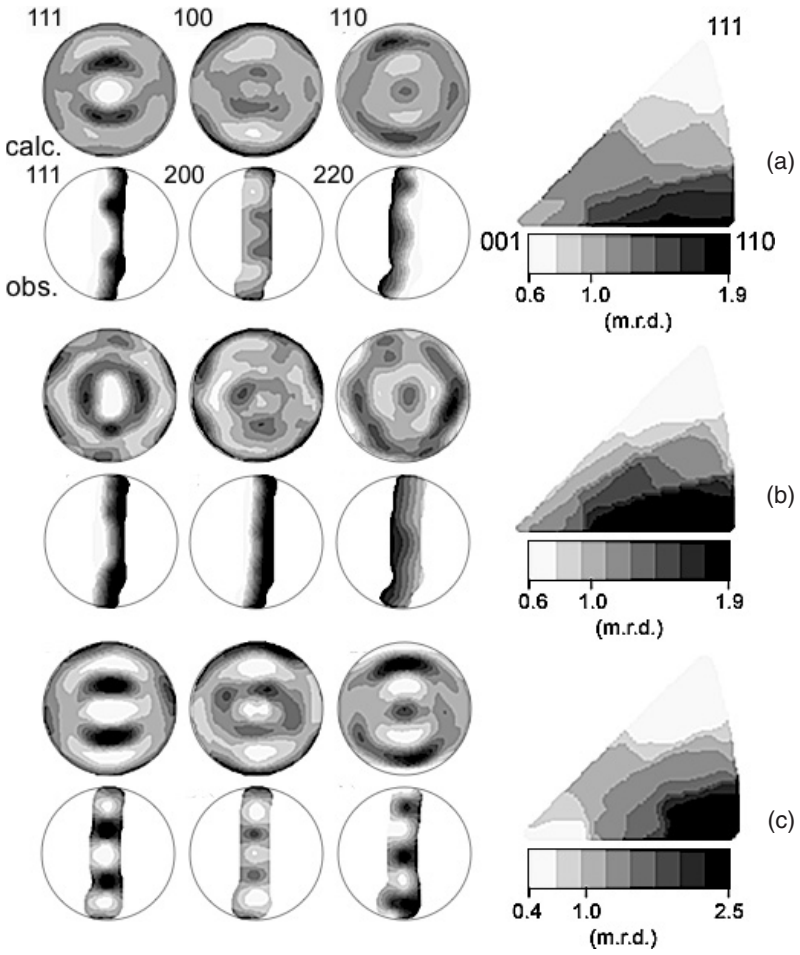

Figure 3. Pole figures of the (111), (100), and (110) crystallographic planes calculated from the OD, experimental pole figures, and inverse pole figure of the compression direction. (a) Copper-1 at 24 ± 2 GPa; (b) Copper-2 at 16 ± 2 GPa; (c) Copper-3 at 24 ± 2 GPa. All the pole figures are plotted in equal area projection.

compression texture is again attributed to 'curling'. The complicated pattern of textures observed for copper, a soft fcc metal, which supports a very small (<0.5 GPa) deviatoric stress throughout all the experiments (see table 2), can be relevant for the interpretation of occasional unusual deformation textures observed in gold, when used as a pressure and position marker in DAC deformation experiments conducted on much stronger silicates and oxides [9].

In addition, we should consider that by scanning the sample across its radial extension with an x-ray beam of finite width smaller than the sample diameter, at each step we probe volumes representing different weighted averages of the radial distance (r) and azimuthal orientation (ω). In particular, at the edge of the sample (large r) the probed volume presents a strong preference for orientations perpendicular to the x-ray beam (figure 5). This suggests that even in the case of ideal axially symmetric textures, probing the periphery of the sample could enhance, by geometry, the textural component corresponding to strain in the radial direction perpendicular to the x-ray beam.

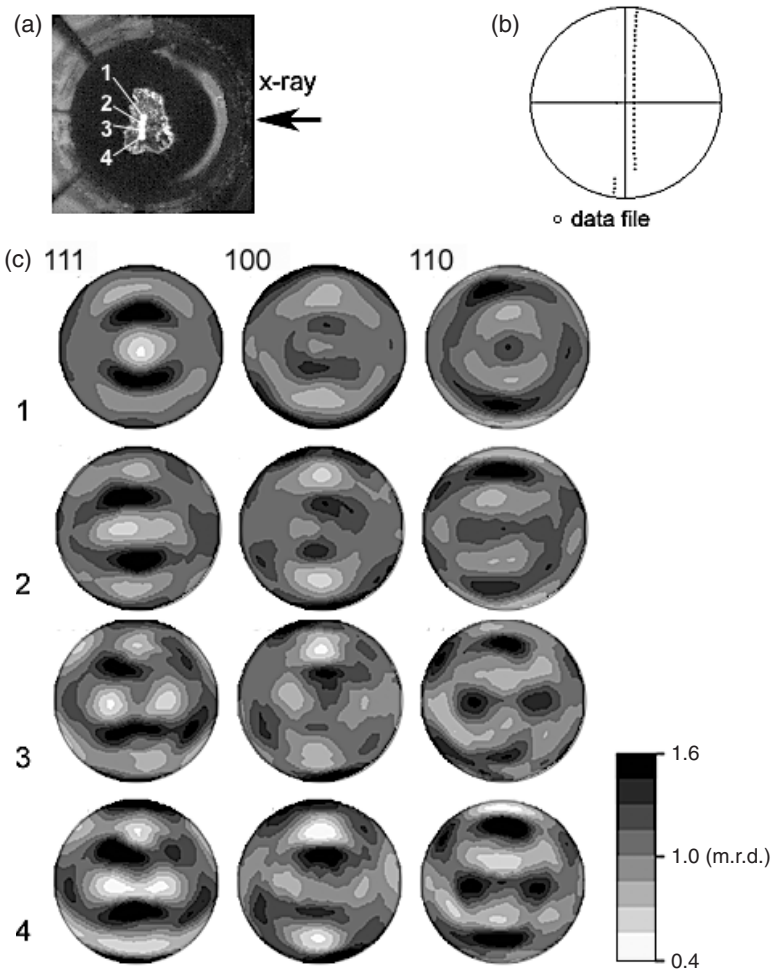

Figure 4. Copper-1 at 24 ± 2 GPa. (a) Image of the sample through the diamond anvil. (b) Experimental data coverage as a stereoplot of the position of the individual 1D spectra (data files) extracted from the 2D diffraction image (equal area projection). (c) (111), (100) and (110) pole figures at selected sample positions at radial distance, r, from the centre of the sample: (1) $r = 0$; (2) $r = 20$ μm; (3) $r = 40$ μm; (4) $r = 60$ μm. Both in the data coverage and the pole figures the compression direction is normal to the figure.

4.2. Experiments in non-ideal stress geometry

In experiments Copper-4 and 5 images contain complete 111, 200, and 220 diffraction rings (figures 2, 6). In both experiments copper is subject to substantial extrusion of the sample in the radial direction. The main difference between the two datasets is caused by the geometry of the sample flow with respect to the x-ray beam direction. In experiment Copper-4 the sample extrudes in a direction close to perpendicular to the x-ray beam, while in Copper-5 the extrusion is in the same direction as the x-ray beam (see figure 7). The experimental geometry for radial diffraction enhances the presence of stress gradients along the x-ray path, because the x-ray beam crosses the whole sample radial extension when the central region of the sample is probed (figure 5).

Table 3. Elastic strain and texture index across a radial scan of Copper-1 at 24 ± 2 GPa and Copper-4 at 21 ± 2 GPa.

Position (r)[a] (μm)	Elastic strain (V/V_0)[b]	Average pressure (GPa)	Min–max texture intensity (mrd)	Texture index (F_2)
Copper-1				
0	0.879	24 ± 2	0.5–1.7	1.4
20	0.873	26 ± 2	0.6–1.7	1.6
40	0.868	28 ± 2	0.4–1.9	2.1
60	0.865	29 ± 2	0.3–2.0	2.4
Copper-4				
0	0.890	21 ± 2	0.4–2.1	1.9
20	0.901	19 ± 2	0.4–2.1	2.3
40	0.909	17 ± 2	0.4–2.5	2.3
60	0.915	15 ± 2	0.3–2.7	3.7
90	0.925	13 ± 2	0.1–2.6	3.8

[a] r is equal to the distance from the centre of the sample.
[b] $V_0 = 47.2299$ Å^3 [11].

Table 4. Elastic strain and texture index of different volumetric component of Copper-5.

Component	Elastic strain (V/V_0)	Average pressure (GPa)	Min–max texture intensity (mrd)	Texture index (F_2)
1	0.951	8 ± 5	0.6–2.1	1.5
2	0.891	21 ± 5	0.6–1.7	1.8
3	0.865	29 ± 5	0.3–2.4	3.2

In experiment Copper-4 the pole figures calculated from the OD show a lack of axial symmetry at the nominal pressure of 21 ± 2 GPa. The pattern of preferred orientation, represented by the (111), (100) and (110) calculated pole figures (figure 7), does not show any significant variation throughout the sample radial extension (from $r = 0$ to 90 μm) except for a rotation, quantified in 25° ± 5°, of the shear direction at 90 μm distance from the centre of the sample (cf figure 7(c)). The results of the texture analysis are reported in table 3. The features of the texture developed in this experiment (figure 7) are very similar to typical rolling textures [13]. Optical observation of the sample assemblage shows extensive plane shearing and sample extrusion outside the original sample chamber and it also confirms the orientation of sample flow as determined by radial x-ray diffraction analysis (figure 7). This is clear evidence that radial diffraction and texture analysis in the diamond-anvil cell can characterize the deformation of the sample and allow us to put constraints on the details in the geometry of the deformation.

In the case of experiment Copper-5, the diffraction data show a large peak broadening, which suggests a strong pressure gradient in the scattering volume, due to the extrusion of the sample in the direction of the x-ray beam (figure 6). The broad x-ray diffraction features are largely asymmetric in shape and they present heterogeneous intensity patterns (figure 6) suggesting that distinct volumetric components of the sample are subject to largely different strains and develop different textures. Based on the features of the broad x-ray peaks, we have arbitrarily selected three high-pressure components (table 4) in the analysis of the data. The quality of the fit is visibly worse than in the other experiments, and our texture determination is only semi-quantitative. The texture developed by the different parts of the sample is not axisymmetric. It is possible to notice a substantial change in the general features of the preferred orientation moving from low strain to high elastic strain regions (identified by the

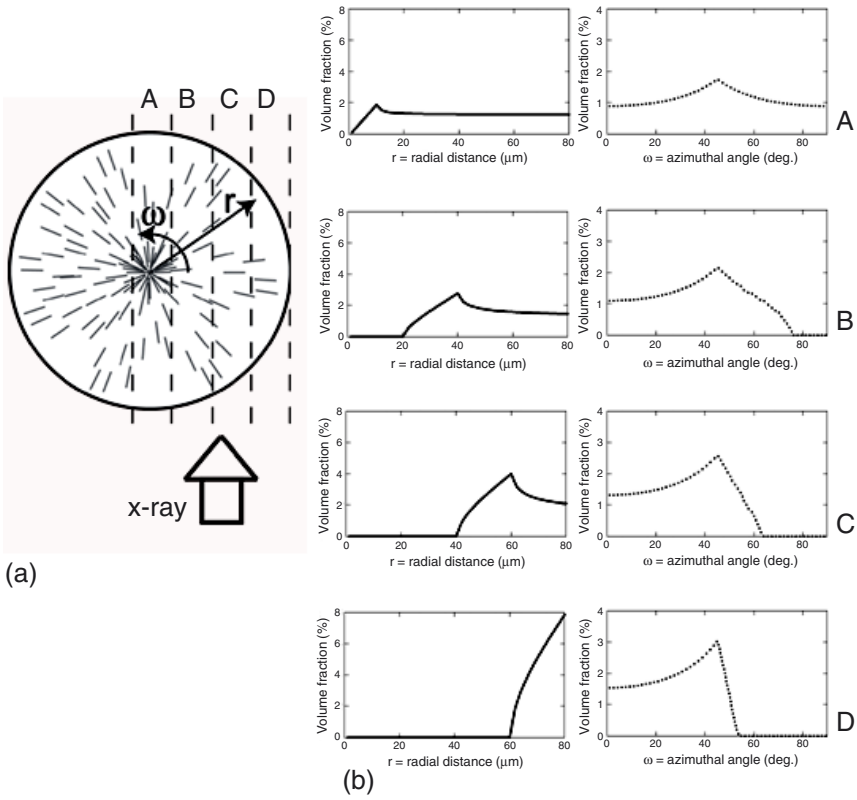

Figure 5. (a) Schematic representation of a transverse section of the sample chamber (diameter = 80 μm). The thin lines represent radial flow lines of a homogeneously axially compressed sample. Each infinitesimal sample element is represented by polar coordinates r (μm) and ω (degree). The x-ray beam of finite horizontal width (20 μm; dashed vertical lines) probes only a portion of the sample. (b) Spectrum of the radial distances and azimuthal orientations expressed as a percentage fraction of the scattering sample volume: (A) case of x-ray beam at $r = 0$; (B) case of x-ray beam at $r = 30$ μm; (C) case of x-ray beam at $r = 50$ μm; (D) case of x-ray beam at $r = 70$ μm. The azimuthal orientations are collapsed to the range $0 \leqslant \omega \leqslant 90°$ because of symmetry. Notice that at large r (edge of the sample) the x-ray probes a very limited range of azimuthal (flow) directions.

large variation of d-spacing for each diffraction line). The combination of the information from the raw data (x-ray diffraction image), and the textural analysis serves as a useful diagnostic of non-ideal sample configuration with flow along the x-ray direction, as confirmed by optical examination of the sample after compression. A quantitative analysis of data collected in the presence of large strain gradients would require a fine experimental characterization and a reliable model of stress/strain distribution in the sample chamber [30–34], which depends not only on geometrical constraints but also on material properties of both the sample and the sample container (both diamond and gasket).

5. Conclusions

Radial x-ray diffraction in the diamond-anvil cell with simultaneous Rietveld refinement and textural analysis represent a viable and promising method to quantitatively analyse plastic deformation of crystalline solids up to pressures comparable to the deep interior of terrestrial

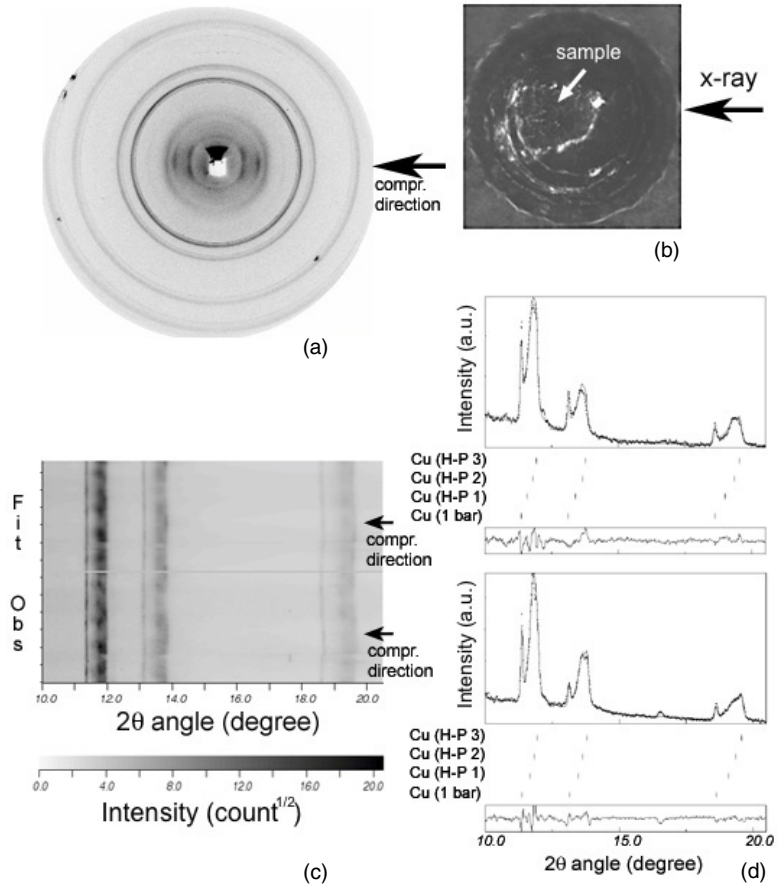

Figure 6. Experimental results for Copper-5. (a) 2D x-ray diffraction image. (b) Image of the sample at the end of the experiment. (c) Map plot of calculated and observed 1D spectral intensities. (d) Representative calculated (line) and observed (dots) 1D spectra in compression and extension directions. Notice the large misfit as shown by the residuals (at the bottom of the plots). In this experiment a signal from copper powder outside the sample chamber (at ambient pressure) was also detected.

planets. Repeated measurements of copper up to 30 GPa at ambient temperature demonstrate the reproducibility of the textural results when the experimental geometry is ideal. The results show a general axisymmetric (110) compression texture comparable with conventional deformation experiments. In the case of non-ideal experimental geometry, both the raw experimental data (images) and the results of the data inversion (pole figures) allow us to quantitatively identify deviations from axial compression geometry. The study of highly ductile copper has revealed considerable heterogeneities in strain inside the diamond-anvil cell. Analogous studies with much harder oxides [35] and silicates [36, 37] indicated fairly homogeneous textures with small strain gradients and approximately axial symmetry. This indicates that caution is required for DAC deformation experiments of soft metals. As a general rule examination of the sample geometry and its evolution during and after compression, by optical observation as well as x-ray transmission profiles (e.g. [8]), furnishes an invaluable diagnostic tool that should always accompany the data analysis in radial DAC experiments. The overall picture emerging from these new results for copper can help to better interpret some

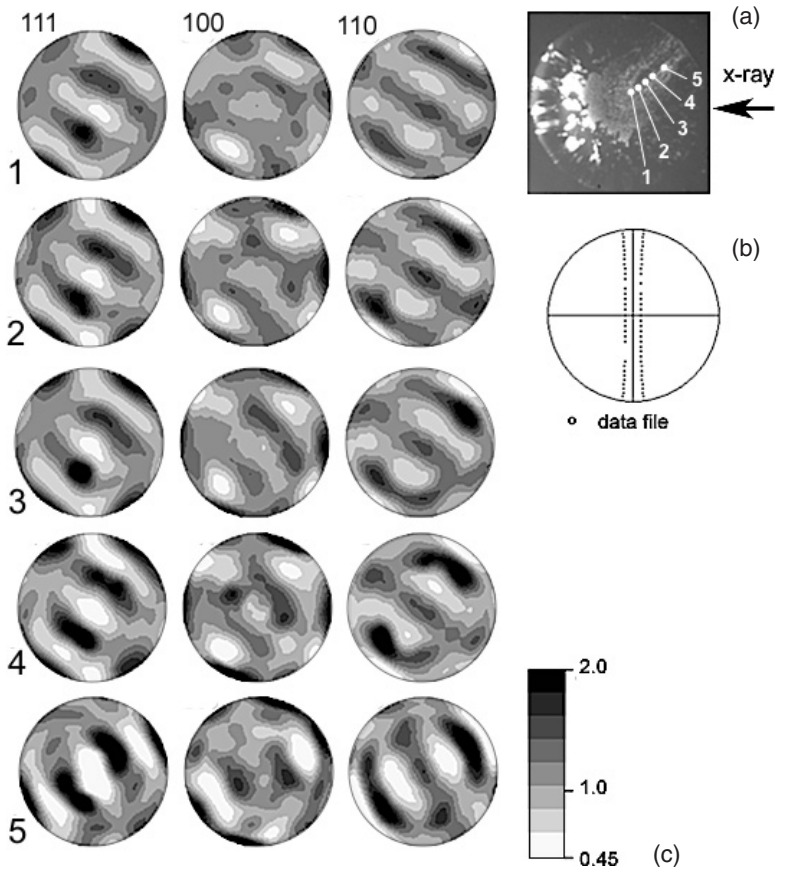

Figure 7. Copper-4 at 21 ± 2 GPa. (a) Image of the sample through the diamond anvil. (b) Experimental data coverage. (c) (111), (100) and (110) pole figures at selected radial distances, r, from the centre of the sample: (1) $r = 0$; (2) $r = 20$ μm; (3) $r = 40$ μm; (4) $r = 60$ μm; (5) $r = 90$ μm. Both in the data coverage and the pole figures the compression direction is normal to the figure.

anomalous texture features observed in gold when used as a marker in other DAC deformation experiments.

Acknowledgments

This research is supported by CDAC. SS is supported by the Miller Institute for Basic Research in Science. GSECARS is supported by the NSF, DOE, and the State of Illinois. HPCAT is supported by DOE-BES, DOE-NNSA (CDAC), NSF, DOD-TACOM, and the WM Keck Foundation. Use of APS was supported by the US DOE-S, DOE-BES. The Advanced Light Source is supported by the Director, Office of Science, Office of Basic Energy Sciences, Materials Sciences Division, of the US Department of Energy under contract No. DE-AC03-76SF00098 at Lawrence Berkeley National Laboratory. The authors thank G Shen, V Prakapenka of the GSECARS at APS, H Liu and M Sommayazulu of HP-CAT at APS, and M Kunz, W A Caldwell, and S M Clark of the beamline 12.2.2 at ALS for their technical support.

References

[1] Williams Q and Jeanloz R 1991 Ultra-high pressure experimental techniques *Molten Salt Techniques* vol 4, ed R J Gale and D G Lovering (New York: Plenum Publishing Corporation) pp 193–227

[2] Duffy T S 2005 Synchrotron facilities and the study of the Earth's deep interior *Rep. Prog. Phys.* **68** 1811–59

[3] Singh A K and Kennedy G C 1974 Uniaxial stress component in tungsten carbide anvil high-pressure x-ray cameras *J. Appl. Phys.* **45** 4686–91

[4] Kinsland G L and Bassett W A 1976 Modification of the diamond cell for measuring strain and the strength of materials at pressures up to 300 kilobar *Rev. Sci. Instrum.* **47** 130–3

[5] Mao H K, Hemley R J and Mao A L 1997 Diamond-cell research with synchrotron radiation *Advances in High Pressure Research in Condensed Matter* ed S K Sikka (New Delhi: NISCOM) pp 12–9

[6] Merkel S, Wenk H S, Shu J, Shen G, Gillet Ph, Mao H K and Hemley R J 2002 Deformation of polycrystalline MgO at pressures of the lower mantle *J. Geophys. Res.* **107** 2271 (doi:10.1029/2001JB000920)

[7] Lin J F, Shu J, Hemley R S, Mao H K and Shen G 2003 Amorphous boron gasket in diamond anvil cell research *Rev. Sci. Instrum.* **74** 4732–6

[8] Merkel S and Yagi T 2005 X-ray transparent gasket for diamond anvil cell high pressure experiments *Rev. Sci. Instrum.* **76** 046109 (doi:10.1063/1.1884195)

[9] Wenk H R, Lonardelli I, Pehl J, Devine J, Prakapenka V, Shen G and Mao H K 2004 In situ observation of texture development in olivine, ringwoodite, magnesiowüstite and silicate perovskite at high pressure *Earth Planet. Sci. Lett.* **226** 507–19

[10] Takemura K 2001 Evaluation of the hydrostaticity of a helium-pressure medium with powder x-ray diffraction techniques *J. Appl. Phys.* **89** 662–8

[11] Dewaele A, Luobeyre P and Mezouar M 2004 Equations of state of six metals above 94 GPa *Phys. Rev.* B **70** 094112

[12] Ahrens T J and Johnson M L 1995 Shock wave data for minerals *Mineral Physics and Crystallography: A Handbook of Physical Constants* (*AGU Reference Shelf* vol 2) ed T J Ahrens (Washington, DC: American Geophysical Union) pp 143–84

[13] Rollett A D and Wright S I 2000 Typical textures in metals *Texture and Anisotropy. Preferred Orientations in Polycrystals and Their Effect on Material Properties* 2nd paperback edn ed U F Kocks, C N Tomé and H R Wenk (Cambridge: Cambridge University Press) pp 185–238

[14] Stout M G, Kallend J S, Kocks U F, Przystupa M A and Rollett A D 1988 Material dependence of deformation texture development in various deformation modes *8th Int. Conf. on Textures of Materials* ed J S Kallend and G Gottstein (Warrendale, PA: The Metallurgical Society) pp 479–84

[15] Holzapfel W B, Hartwig M and Sievers W 2001 Equation of state for Cu, Ag, and Au for wide ranges in temperature and pressure up to 500 GPa and above *J. Chem. Phys. Ref. Data* **30** 516–29

[16] Mao H K, Kao C and Hemley R J 2001 Inelastic x-ray scattering at ultrahigh pressures *J. Phys.: Condens. Matter* **13** 7847–58

[17] Kunz M, MacDowell A A, Caldwell W A, Cambie D, Celestre R S, Domning E E, Duarte R M, Gleason A E, Glossinger J M, Kelez N, Plate D W, Yu T, Zang J M, Padmore H A, Jeanloz R, Alivisatos A P and Clark S M 2005 *J. Synchrotron Radiat.* **12** 650–8

[18] Hammersley A P 1998 *FIT2D: V99129 Reference Manual Version 3.1 (Internal Report* ESRF-98-HA01) (Grenoble, France: ESRF)

[19] Lutterotti L, Matthies S, Wenk H R, Schultz A S and Richardson J W Jr 1997 Combined texture and structure analysis of deformed limestone from time-of-flight neutron diffraction spectra *J. Appl. Phys.* **81** 594–600

[20] Rietveld H M 1969 A profile refinement method for nuclear and magnetic structures *J. Appl. Crystallogr.* **2** 65–72

[21] Matthies S 2002 20 years of WIMV, history, experience and contemporary developments *Mater. Sci. Forum* **228** 83–8

[22] Lonardelli I, Wenk H R, Lutterotti L and Goodwin M 2005 Texture analysis from synchrotron diffraction images with the Rietveld method: dinosaur tendon and salmon scale *J. Synchrotron Radiat.* **12** 354–60

[23] Ischia G, Wenk H R, Lutterotti L and Berberich F 2005 Quantitative Rietveld texture analysis of zirconium from single synchrotron diffraction images *J. Appl. Crystallogr.* **38** 377–80

[24] Heinz D L and Jeanloz R 1984 The equation of state of the gold calibration standard *J. Appl. Phys.* **55** 885–93

[25] Duffy T S, Shen G, Heinz D L, Shu J, Ma Y, Mao H K, Hemley R J and Singh A K 1999 Lattice strains in gold and rhenium under nonhydrostatic compression to 37 GPa *Phys. Rev.* B **60** 15063–73

[26] Daniels W B and Smith C S 1958 Pressure derivatives of the elastic constants of copper, silver, and gold to 10000 bars *Phys. Rev.* **111** 713–21

[27] Karki B B, Stixrude L and Wentzcovitch R M 2001 High-pressure elastic properties of major materials of Earth's mantle from first principles *Rev. Geophys.* **39** 507–34

[28] Singh A K 1993 The lattice strains in a specimen (cubic system) compressed nonhydrostatically in an opposed anvil device *J. Appl. Phys.* **73** 4278–88
[29] Hosford W F Jr 1964 Microstructural changes during deformation of [011] fiber-textured metals *Trans. Metall. Soc. AIME* **230** 12–5
[30] Sung C M, Goetze C and Mao H K 1977 Pressure distribution in the diamond anvil press and the shear strength of fayalite *Rev. Sci. Instrum.* **48** 1386–91
[31] Moss W C, Hallquist J O, Reichlin R, Goettel K A and Martin S 1986 Finite element analysis of the diamond anvil cell: Achieving 4.6 Mbar *Appl. Phys. Lett.* **48** 1258–60
[32] Meade C and Jeanloz R 1988 Yield strength of MgO to 40 GPa *J. Geophys. Res.* **93** 3261–9
[33] Ruoff A L and Luo H 1991 Pressure strengthening: A possible route to obtaining 9 Mbar and metallic diamonds *J. Appl. Phys.* **70** 2066–70
[34] Merkel S, Hemley R J and Mao H K 1999 Finite-element modeling of diamond deformation at multimegabar pressures *Appl. Phys. Lett.* **74** 656–8
[35] Tommaseo C E, Devine J, Merkel S, Speziale S and Wenk H R 2005 Texture development and elastic stresses in magnesiowüstite at high pressure *Phys. Chem. Miner.* **33** 84–97
[36] Miyagi L, Merkel S, Yagi T, Sata N, Ohishi Y and Wenk H R 2006 Quantitative Rietveld analysis of $CaSiO_3$ perovskite deformed in the diamond anvil cell *J. Phys.: Condens. Matter* **18** S995–1005
[37] Wenk H R, Lonardelli I, Merkel S, Miyagi L, Pehl J, Speziale S and Tommaseo C E 2006 Deformation textures produced in radial diamond anvil cell experiments *J. Phys.: Condens. Matter* **18** S933–47
[38] Bunge H J 1982 *Texture Analysis in Materials Science-Mathematical Methods* (London: Butterworths)